



BRILL

*Multidiscipline Modeling in Mat. and Str.* 4(2008)XX-XX

MMMS

www.brill.nl/mmms

# A COMBINED MULTI-MATERIAL EULER/LAGRANGE COMPUTATIONAL ANALYSIS OF BLAST LOADING RESULTING FROM DETONATION OF BURIED LANDMINES

M. Grujicic<sup>1</sup>, B. Pandurangan<sup>1</sup>, G. M. Mocko<sup>1</sup>, S. T. Hung<sup>1</sup>, B. A. Cheeseman<sup>2</sup>, W. N. Roy<sup>2</sup>  
and R. R. Skaggs<sup>2</sup>

<sup>1</sup>Department of Mechanical Engineering Clemson University, Clemson SC 29634

<sup>2</sup>Army Research Laboratory – Survivability Materials Branch Aberdeen, Proving Ground, MD 21005-5069

mica.grujicic@ces.clemson.edu

Received 26 November 2006; accepted 10 March 2007

---

## Abstract

Detonation of landmines buried to different depths in water-saturated sand is analyzed computationally using transient non-linear dynamics simulations in order to quantify impulse loading. The computational results are compared with the corresponding experimental results obtained using the Vertical Impulse Measurement Fixture (VIMF), a structural mechanical device that enables direct experimental determination of the blast-loading impulse. The structural-dynamic/ballistic response of the Rolled Homogenized Armor (RHA) used in the construction of the VIMF witness plate and the remainder of the VIMF and the hydrodynamic response of the TNT high-energy explosive of a mine and of the air surrounding the VIMF are represented using the standard materials models available in literature. The structural-dynamic/ballistic response of the sand surrounding the mine, on the other hand, is represented using our recent modified compaction model which incorporates the effects of degree of saturation and the rate of deformation, two important effects which are generally neglected in standard material models for sand.

The results obtained indicate that the use of the modified compaction model yields a substantially better agreement with the experimentally-determined impulse loads over the use of the original compaction model. Furthermore, the results suggest that, in the case of fully saturated sand, the blast loading is of a bubble type rather than of a shock type, i.e. the detonation-induced momentum transfer to the witness plate is accomplished primarily through the interaction of the sand-over-burden (propelled by the high-pressure expanding gaseous detonation by-products) with the witness plate.

## Keywords

Detonation, Shallow Buried Mine, Blast Loading, AUTODYN

## NOMENCLATURE

## Report Documentation Page

Form Approved  
OMB No. 0704-0188

Public reporting burden for the collection of information is estimated to average 1 hour per response, including the time for reviewing instructions, searching existing data sources, gathering and maintaining the data needed, and completing and reviewing the collection of information. Send comments regarding this burden estimate or any other aspect of this collection of information, including suggestions for reducing this burden, to Washington Headquarters Services, Directorate for Information Operations and Reports, 1215 Jefferson Davis Highway, Suite 1204, Arlington VA 22202-4302. Respondents should be aware that notwithstanding any other provision of law, no person shall be subject to a penalty for failing to comply with a collection of information if it does not display a currently valid OMB control number.

1. REPORT DATE

**2008**

2. REPORT TYPE

3. DATES COVERED

**00-00-2008 to 00-00-2008**

4. TITLE AND SUBTITLE

**A Combined Multi-Material Euler/LaGrange Computational Analysis of Blast Loading Resulting from Detonation of Buried Landmines**

5a. CONTRACT NUMBER

5b. GRANT NUMBER

5c. PROGRAM ELEMENT NUMBER

6. AUTHOR(S)

5d. PROJECT NUMBER

5e. TASK NUMBER

5f. WORK UNIT NUMBER

7. PERFORMING ORGANIZATION NAME(S) AND ADDRESS(ES)

**Celmsom University, Department of Mechanical Engineering, Clemson, SC, 29634**

8. PERFORMING ORGANIZATION REPORT NUMBER

9. SPONSORING/MONITORING AGENCY NAME(S) AND ADDRESS(ES)

10. SPONSOR/MONITOR'S ACRONYM(S)

11. SPONSOR/MONITOR'S REPORT NUMBER(S)

12. DISTRIBUTION/AVAILABILITY STATEMENT

**Approved for public release; distribution unlimited**

13. SUPPLEMENTARY NOTES

**Multidiscipline Modeling in Materials and Structures, 4, pp. 105-124, 2008.**

14. ABSTRACT

**Detonation of landmines buried to different depths in water-saturated sand is analyzed computationally using transient non-linear dynamics simulations in order to quantify impulse loading. The computational results are compared with the corresponding experimental results obtained using the Vertical Impulse Measurement Fixture (VIMF), a structural mechanical device that enables direct experimental determination of the blast-loading impulse. The structural-dynamic/ballistic response of the Rolled Homogenized Armor (RHA) used in the construction of the VIMF witness plate and the remainder of the VIMF and the hydrodynamic response of the TNT high-energy explosive of a mine and of the air surrounding the VIMF are represented using the standard materials models available in literature. The structural-dynamic/ballistic response of the sand surrounding the mine, on the other hand, is represented using our recent modified compaction model which incorporates the effects of degree of saturation and the rate of deformation, two important effects which are generally neglected in standard material models for sand. The results obtained indicate that the use of the modified compaction model yields a substantially better agreement with the experimentally-determined impulse loads over the use the original compaction model. Furthermore, the results suggest that, in the case of fully saturated sand, the blast loading is of a bubble type rather than of a shock type, i.e. the detonation-induced momentum transfer to the witness plate is accomplished primarily through the interaction of the sand-over-burden (propelled by the high-pressure expanding gaseous detonation by-products) with the witness plate.**

15. SUBJECT TERMS

16. SECURITY CLASSIFICATION OF:			17. LIMITATION OF ABSTRACT <b>Same as Report (SAR)</b>	18. NUMBER OF PAGES <b>28</b>	19a. NAME OF RESPONSIBLE PERSON
a. REPORT <b>unclassified</b>	b. ABSTRACT <b>unclassified</b>	c. THIS PAGE <b>unclassified</b>			

**Standard Form 298 (Rev. 8-98)**  
Prescribed by ANSI Std Z39-18

$A$	-	Constant in JWL Equation of State
$\alpha$	-	Porosity
$B$	-	Compaction Modulus
$B_1$	-	Constant in JWL Equation of State
$\beta$	-	Saturation ratio
$E$	-	Internal energy
$\gamma$	-	Constant-Pressure to constant-volume specific heats ratio
$\gamma_1$	-	Saturation Parameter
$K$	-	Bulk Modulus
$\mu$	-	Compression ratio
$P$	-	Pressure
$R_1$	-	Constant in JWL Equation of State
$R_2$	-	Constant in JWL Equation of State
$\rho$	-	Density
$v$	-	Specific volume
$V$	-	Volume
$w$	-	Constant in JWL Equation of State
$x$	-	Spatial coordinate
$y$	-	Spatial coordinate

### *Subscripts*

$MC$	-	Mohr-Coulomb value
$p$	-	Pore related quantity
$s$	-	Fully-compacted sand related quantity
$sat$	-	Saturation related quantity
$w$	-	Water related quantity
$Comp$	-	Value at full compaction
$dry$	-	Dry Sand quantity
$o$	-	Initial value
$p$	-	Pore related quantity
$pl$	-	Plastic state quantity
$Pl.Comp$	-	Plastic Compaction related quantity
$s$	-	Fully-compacted sand related quantity
$Solid.Comp$	-	Solid Compaction related quantity
$H$	-	Homologous quantity
$Unsat$	-	Unsaturated Sand related quantity

### *Superscripts*

*	-	Value at minimum pressure for full sand compaction
---	---	--

## 1. INTRODUCTION

Buried explosives such as land mines and improvised explosive devices are a constant threat to the US Military vehicles. Since World War II, buried explosives have caused the destruction of more military vehicles than all the threats combined [1]. Yet, mine

survivability is one of the least understood subjects related to the design and manufacture of military vehicles, in particular, the fundamentals governing a landmine blast and the interactions between the detonation byproducts and soil ejecta with the target vehicles resulting in the vehicle damage/destruction are poorly understood. Typically, enhanced mine survivability of the vehicles is attained through the use of heavier armor.

The most common used landmines are the so called "*blast mines*" which contain a large amount of explosive and produce the damage/destruction of the target by blast loading. While the landmines represent a serious threat to light or unprotected vehicles, "*shaped charges*" and "*penetrator mines*" are typically required to inflict damage on the heavy armored vehicles. Shaped charges which consist of a ductile-metal inverted cone surrounded by a jacket of high-energy explosive produce a hot jet of molten metal after detonation of the explosive. The molten-metal jet is capable of penetrating a steel armor several inches in thickness. Penetrator mines on the other hand, compromise the integrity of the armor by impacting it with a projectile. Since the shaped charges and penetrator mines are not the subject of the present work they will not be considered any further.

Detonation is a process in which as the pressure wave propagates through the explosive, chemical reactions are initiated behind the pressure wave. These reactions give rise to a rapid release of energy in the form of a shock wave and to a slower release of energy in the form of an expanding gas bubble. Initial pressures as high as 200,000 atmospheres and initial temperatures as high as 6000°C can be often found near the detonation point. Detonation of an explosive buried in soil is typically considered to consist of three different phases (a) the detonated explosive/soil interaction phase; (b) gaseous detonation products expansion phase, and (c) detonation-products/vehicle and soil-ejecta/vehicle interaction phase.

Within the first phase mentioned above, the detonation wave of the explosive produces a shock wave in the surrounding soil [1]. When the shockwave traveling through the soil reaches the soil/air interface, it reflects, to a large extent, back into the soil (but as an expansion wave. In addition, a small fraction of the incident shock wave is transmitted into the air and a thin top layer of soil is ejected upward. In other words, a large difference in the acoustic impedance between the soil and air causes the shock wave to produce only a minor loading on the target structure (unless the target structure is very near the soil/air interface) [2].

In the second phase, gaseous detonation products undergo volumetric expansion producing mechanical work, the magnitude of which scales with the mass of the explosive. In the case of the explosives shallow-buried in soil, the expansion of detonation products takes place predominantly in the upward direction giving rise to the formation of a soil-overburden bubble [2]. The continuing expansion of detonation products ultimately causes the fracture of the soil bubble and the ejection of a soil plug into the air and the creation of a bow shock wave. It is generally accepted that the associated venting of high-dynamic pressure detonation products can cause localized deformation of the target. When the expanding gases are confined by the soil and the target, they can produce dynamic loading over a larger area of the target. It should be noted that the angular distribution of the detonation-products expansion is greatly affected by the properties of the soil and the depth of burial of the explosive. While the initial expansion of the detonation products causes the soil directly above the charge to

rapidly move upward, the interaction of the expanding gas with the surrounding soil causes the soil to flow (and to be ultimately ejected) as an annulus surrounding the expanding detonation products [2].

In the third phase, the gaseous detonation product-target/soil ejecta-target interaction phase two main dynamic loading mechanisms are typically considered: (a) short-duration concentrated impact loading resulting from the interaction of the ejected soil plug and the blast high-pressure detonation products with the target structure; and (b) long duration distributed dynamic loading dominated by the interactions between soil ejecta and the target structure.

A schematic representing the different stages of detonation of a landmine is shown in Figs.1(a)-1(f). The first stage of detonation is depicted in Fig.1(a) and involves interactions between the exploded landmine and the soil resulting in the shock formation in the soil and soil melting/vaporization. The second stage is depicted in Figs.1(b)-1(d). In Fig. 1(b), a spherical shock wave reaches the soil/air interface causing soil spalling while the spherically-shaped landmine cavity grows. In Fig.1(c), the rarefaction wave, generated on the soil /air interface reaches the landmine cavity causing it to expand preferentially in the upward direction. Continued expansion of the cavity causes the formation, growth and ultimate rupture of a sand-overburden mound, Fig.1(d). This in turn gives rise to initial venting of the gaseous detonation products. The third stage of landmine detonation is depicted in Fig.1(e)-1(f) where a massive venting of the detonation products, ejection of sand and formation of crater can be observed.

The design of survivable vehicles and platforms (targets) requires the ability to understand and quantify the impulsive detonation loads from the landmines buried in different soil media and to model the response of structures/targets of interest. Elucidation and quantification of the (time-dependent) load a buried landmine applies to a target structure above it when the landmine is detonated (typically represented by the associated total vertical impulse or by the spatial distribution of the specific impulse) is quite challenging since such load depends on the size and shape of the charge, its depth of burial, the distance between the soil surface and the target, and the properties (density, particle size and distribution, presence of organic matter, water content, etc.) of the soil in which the landmine is buried. Direct experimental characterizations of landmine-blast events are highly critical for getting a better understanding of the accompanying enormously complex phenomena. However, it is not practical or cost-effective to carry out experimental determination of the response of all targets of interest to buried charges of all sizes in a variety of soils. Recent advances in numerical analysis capabilities, particularly the coupling of Eulerian solvers (used to model gaseous detonation products and air) and Lagrangian solvers (used to represent vehicles/platforms and soil), have allowed simulations to provide insight into complex loading created by the mine blast event. However, a quantified understanding of the blast phenomena and loadings through computer modeling is still not mature. As discussed in our previous work [3], the lack of maturity of computer simulations of the blast event is mainly due to inability of the currently available materials models to realistically represent the response of the materials involved under high-deformation, high deformation-rate, high-temperature conditions, the type of conditions accompanying landmine detonation. In particular, the soil response and its dependence on the soil composition, microstructure and water content are poorly understood [4].

A review of the literature shows that there exists an extensive body of work dealing with the investigation of buried charges. However, much of this work does not focus on the characterization of the blast output of landmines, but rather on cratering effects in soils, with applications towards the efficient utilization of explosives for excavation (i.e. canals, trenches, etc.) or in the survivability of structures subjected to near surface blasts [4].

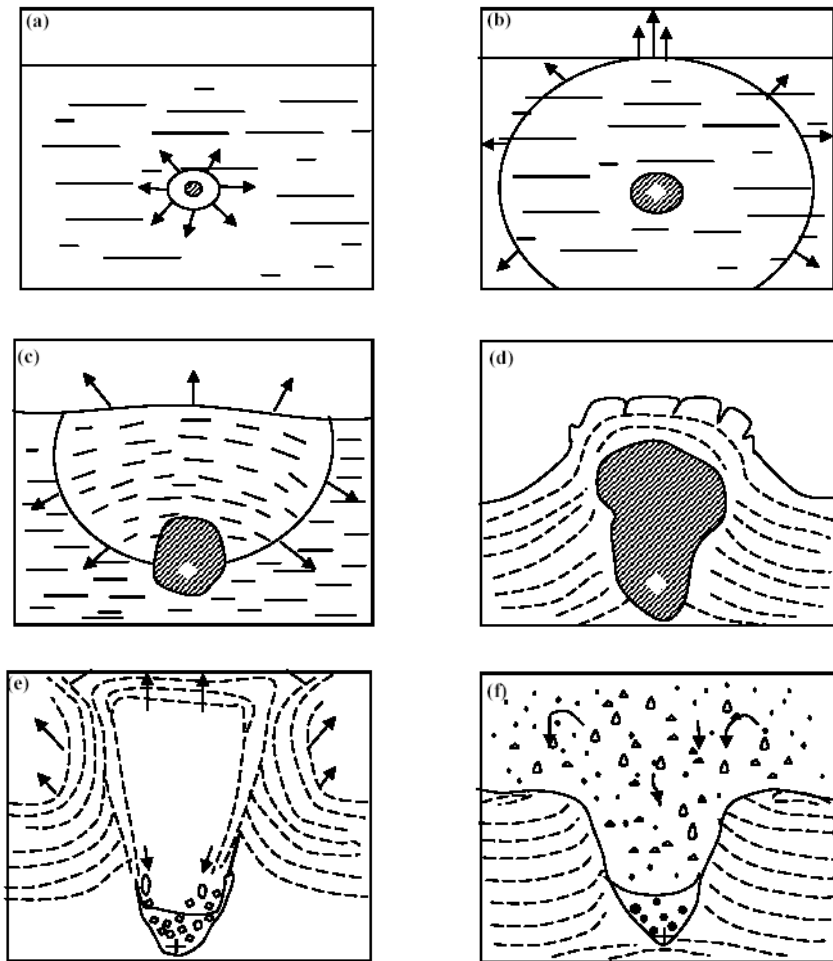


**Fig.1** Various stages of detonation of a landmine shallow buried in sand.  
Please see text for details.

Among the works published in the open literature which directly deal with experimental characterization of the effects of anti-tank (AT) and anti-personnel (AP) landmine blasts, the following appear to be the most relevant to the present subject matter. Westine et al. [5] carried out experiments on a plate which was mounted above a buried charge representing an AT landmine. The plate contained a number of through-the-thickness holes at incremental distances from the mine, in which, plugs of known mass were placed. The blast accompanying mine detonation caused the plugs to be

driven out of the holes and from their velocity the impulsive loading on the plate was calculated. Morris [6] used the results of Westine et al. [5] to construct a design-for-survivability computer code for lightweight vehicles. More recently, Bergeron et al. [7] carried out a comprehensive investigation of the buried landmine blasts using an instrumented ballistic pendulum. From these experiments, the pressure and impulse as a function of time were recorded at several locations in air directly above the mine as well as in the sand surrounding the mine, along with x-radiographs and high speed photographs of the associated soil cratering and ejecting phenomena. The work of Bergeron et al. [7] was subsequently extended by Braid [8] to incorporate different charge sizes, soil types and improved instrumentation.

In our recent computational work [3] based on the use of AUTODYN, a general-purpose transient non-linear dynamics explicit simulation software [9], a detailed comparison was made between the experimental results of Bergeron et al. [10] and their computational counterparts for a number of detonation-related phenomena such as the temporal evolutions of the shape and size of the over-burden sand bubbles and of the detonation-products gas clouds, the temporal evolutions of the side-on pressures in the sand and in air, etc. It was found that the most critical factor hampering a better agreement between the experiment and computational analysis is an inadequacy of the current material models for sand to capture the dynamic response of this material under blast loading conditions. Hence, the main objective of our subsequent work [11] was to improve the compaction materials model for sand in order to include the effects of the degree of saturation and rate of deformation, the two important effects which were neglected in the available constitutive models for sand. The new material constitutive model for sand was subsequently validated for the case of sand with a low level of water saturation by comparing the experimental results associated with detonation of the shallow-buried and ground-laid C4 mines obtained through the use of an instrumented horizontal mine-impulse pendulum with their computational counterparts obtained via detailed numerical modeling of the same physical problem using AUTODYN. In our follow-up work [12], the newly developed materials constitutive model for sand was used within a transient non-linear dynamics computational analysis to predict the effect of detonation associated with mines buried in fully water-saturated sand. The computational results obtained were compared with their experimental counterparts reported in the work of Taylor and Skaggs [13] who carried out large-scale experiments using the Vertical Impulse Measurement Fixture (VIMF) at the Army Research Laboratory, Aberdeen, MD. The VIMF is a unique facility that has been designed specifically to measure accurately the vertical impulse from buried charges weighing up to 8 kg.

In our computational analysis presented in Ref. [12], a simplified single-phase Euler-FCT model was used to represent the gaseous detonation products and air. In the present work, a more accurate multi-material Euler model is used to represent the two gaseous materials at hand.

The organization of the paper is as follows. A brief overview of the design, construction and performance of the Vertical Impulse Measurement Fixture (VIMF) is given in Section II.1. The non-linear dynamics approach, the relevant materials models and the definition of the computational problem investigated are respectively discussed in Sections II.2, II.3 and II.4. The results obtained in the present work are presented and discussed in Section III. The main conclusions resulting from the present work are

summarized in Section IV.

## II. COMPUTATIONAL PROCEDURE

### II.1 An Overview of the Vertical Impulse Measurement Fixture (VIMF)

The VIMF is a structural mechanical device that enables direct experimental determination of the imparted blast-loading impulse via measurements of the vertical displacement of a known fixed-mass vertical guide rail that is capped with a witness plate, which serves as a momentum trap to capture the blast loading of the buried charge. The design and operation of the VIMF has been described in details by Gniazdowski et al. [14], and Skaggs et al. [15] and Taylor and Skaggs [13] and will be only briefly discussed here. A schematic drawing of the VIMF including the vertical guide rail and the orientation of the charge in the water-saturated sand is shown in Fig.2. To create the required water-saturated sand condition, a cylindrical pit 3.65m in diameter and 1.32m deep is first constructed in the soil within the VIMF test area. To retain water in the sand pit and to keep the sand-water mixture separate from the rest of the sand, the walls of the pit are lined with 0.32cm thick poly-ethylene sheets and the pit floor is built using a commercial swimming pool liner. Once the pit liners are in place, a series of water hoses is placed in pit bottom to allow the introduction of water into the pit from the bottom. Next, approximately 14.2m<sup>3</sup> of commercially available (Quickrete) sand is placed in the pit. The sand typically consists of 94.4% sand, 0.3% gravel, and 5.3% silt/clay. The maximum dry-sand density is 1.49 g/cm<sup>3</sup> while the maximum wet-sand density is 1.91 g/cm<sup>3</sup>. Prior to each test, water is allowed to fill the sand pit until standing water is observed on top of the sand.

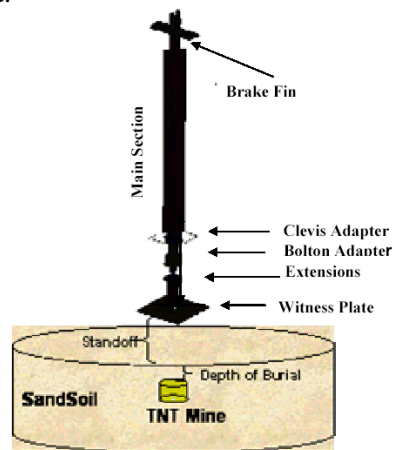


**Fig.2** The Vertical Impulse Measurement Fixture (VIMF).

### II.2 Non-linear Dynamics Modeling of Detonation Phenomena

All the calculations carried out in the present work were done using AUTODYN, a general purpose non-linear dynamics modeling and simulation software [10]. In this section, a brief overview is given of the basic features of AUTODYN, emphasizing the

aspects of this computer program which pertain to the problem at hand and which were not discussed in our previous work [3, 9].

A transient non-linear dynamics problem is analyzed within AUTODYN by solving simultaneously the governing partial differential equations for the conservation of momentum, mass and energy along with the materials constitutive equations and the equations defining the initial and the boundary conditions. The equations mentioned above are solved numerically using a second-order accurate explicit scheme and one of the two basic mathematical approaches, the Lagrange approach and the Euler approach. Within AUTODYN these approaches are referred to as "*processors*". The key difference between the two basic processors is that within the Lagrange processor the numerical grid is attached to and moves along with the material during calculation while within the Euler processor, the numerical grid is fixed in space and the material moves through it. In our recent work [12], a brief discussion was given of how the governing differential equations and the materials constitutive models define a self-consistent system of equations for the dependent variables (nodal displacements, nodal velocities, cell material densities and cell internal energy densities).

In the present work, both the Lagrange and Euler processors are used. The Lagrange processor was used to model the sand and all the structural components of the Vertical Impulse Measurement Fixture (VIMF). The gaseous mine-detonation products and the air surrounding the VIMF are modeled using the multi-material Euler processor. Different regions of the mine/air/VIMF/sand model are allowed to interact and self-interact using the AUTODYN interaction options. A brief overview of the parts interactions and self interactions AUTODYN algorithms can be found in our recent work [12].

Since a brief overview of the Lagrange processor (including the use of cell-erosion mechanism) can be found in our recent work [12], only the multi-material Euler processor will be discussed in the remainder of this section. As discussed earlier, since several materials may simultaneously reside within a single computational cell, the multi-material Euler scheme of AUTODYN was used in the present work. Within this scheme, a control volume method is used to solve the integral and finite-difference forms of the mass, momentum and energy conservation equations in order to obtain an accurate and stable solution. The terms appearing in these equations are divided into two groups: Lagrangian and transport (convective). A two-step numerical procedure is used to solve the finite-difference form of the governing equations. Within the first step, the Lagrange (cell-deforming) step, the Lagrangian form of the governing equations is advanced one time interval. Within the second step, the Euler step, the dependant variables updated in the first step are mapped on to the un-deformed Euler mesh. Multiple materials are handled through a volume fraction technique or an interface technique developed by Young's [16]. All dependent variables are referenced with respect to the center of the cell.

It should be noted that while the Euler formulations are ideally suited for handling large deformations and fluid flow, they suffer from the difficulties in tracking free-surfaces, material interfaces and history-dependent material behavior. The Euler formulation may also be prone to numerical diffusion associated with material convection between cells. Interfaces between the Euler and Lagrange parts were tracked in AUTODYN using the SLIC (Simple Linear Interface Calculation) algorithm developed by Noh and Woodward [27]. Within SLIC, the location of an interface is

tracked separately in each coordinate direction. In other words, the position of the interface in a given direction is determined using the (filled/empty) status of the neighboring cell in that direction. Consequently, the representation of the same interface generally appears to be different in different coordinate directions.

Since the material constitutive models play a dominant role in transient non-linear dynamics analysis like the one associated with mine-detonation, a detailed account of the constitutive models for the materials encountered in the present work is given in the next section.

### II.3 *Materials Constitutive Models*

As discussed in the previous section, the complete definition of a transient non-linear dynamics problem entails the knowledge of the materials models that define the relationships between the flow variables (pressure, mass-density, energy-density, temperature, etc.). These relations typically involve an equation of state, a strength equation and a failure equation for each constituent material. These equations arise from the fact that, in general, the total stress tensor can be decomposed into a sum of a hydrostatic stress (pressure) tensor (which causes a change in the volume/density of the material) and a deviatoric stress tensor (which is responsible for the shape change of the material). An equation of state then is used to define the corresponding functional relationship between pressure, density and internal energy (temperature), while a strength relation is used to define the appropriate equivalent plastic strain, equivalent plastic strain rate, and temperature dependences of the equivalent deviatoric stress. In addition, a materials model generally includes a failure criterion, i.e. an equation describing the (hydrostatic or deviatoric) stress and/or strain condition(s) which, when attained, causes the material to fracture and lose its ability to support normal and shear stresses.

In the present work, the following four materials are utilized within the computational domain: air, Rolled Homogenized Armor (RHA), TNT high-energy explosive and sand. In the following sections, a brief description is given of the models used for each of the four constituent materials. The values of the material parameters for air, RHA and TNT defined in the remainder of the section are available in the AUTODYN materials library [10] and are available to the licensed AUTODYN users. The material model parameters for sand can be found in our recent work [9].

#### II.3.1 *Air*

Air is modeled as an ideal gas and, consequently, its equation of state is defined by the ideal-gas gamma-law relation as [10]:

$$P = (\gamma - 1) \frac{\rho}{\rho_0} E \quad (1)$$

where  $P$  is the pressure,  $\gamma$  the constant-pressure to constant-volume specific heats ratio (=1.4 for a diatomic gas like air),  $\rho_0$  (=1.225kg/m<sup>3</sup>) is the initial air mass density, and  $\rho$  is the current density. For Eq. (1) to yield the standard atmosphere pressure of 101.3kPa, the initial internal energy density  $E$  is set to 253.4kJ/m<sup>3</sup> which corresponds to the air mass specific heat of 717.6J/kg·K and a reference temperature of 288.2K.

Since air is a gaseous material and has no ability to support either shear stresses or negative pressures, no strength or failure relations are required for this material.

### II.3.2 Rolled Homogenized Armor (RHA)

As mentioned earlier, the impulse capturing plate of the VIMF is made of RHA. The dynamic mechanical response of this material is modeled in the present work using: (a) a linear equation of state; (b) a Johnson-Cook strength model and (c) a Johnson-Cook failure model. A detailed description of the material model for RHA can be found in our recent work [12].

### II.3.3 TNT

The Jones-Wilkins-Lee (JWL) equation of state is used for TNT in the present work since that is the preferred choice for the equation of state for high-energy explosives in most hydrodynamic calculations involving detonation. The JWL equation of state is defined as [10]:

$$P = A \left( 1 - \frac{w}{R_1 v} \right) e^{-R_1 v} + B_1 \left( 1 - \frac{w}{R_2 v} \right) e^{-R_2 v} + \frac{wE}{v} \quad (2)$$

where the constants  $A$ ,  $R_1$ ,  $B_1$ ,  $R_2$  and  $w$  for TNT are defined in the AUTODYN materials library and  $v$  is the specific volume of the material.

As explained earlier, within a typical hydrodynamic analysis, detonation is modeled as an instantaneous process which converts unreacted explosive into gaseous detonation products and detonation of the entire high-explosive material is typically completed at the very beginning of a given simulation. Consequently, no strength and failure models are required for a high-energy explosive such as TNT.

### II.3.4 Sand

In this section, a brief overview is provided of the material model for sand which was developed in our recent work [9]. Sand has generally a complex structure consisting of mineral solid particles which form a skeleton. The pores between the solid particles are filled with a low-moisture air (this type of sand is generally referred to as “*dry sand*”), with water containing a small fraction of air (“*saturated sand*”) or comparable amounts of water and air (“*unsaturated sand*”). The relative volume fractions of the three constituent materials in the sand (the solid mineral particles, water and air) are generally quantified by the porosity,  $\alpha$ , and the degree of saturation (Saturation Ratio),  $\beta$ , which are respectively defined as:

$$\alpha = \frac{V_p}{V} \quad (3)$$

and

$$\beta = \frac{V_w}{V_p} \quad (4)$$

where  $V_p$  is the volume of void (pores),  $V_w$  is the volume of water and  $V$  is the total volume.

Surface roughness and the presence of inorganic/organic binders are generally considered to be the main causes for friction/adhesion at the inter-particle contacting surfaces. Deformation of the sand is generally believed to involve two main basic mechanisms [17]: (a) elastic deformations (at low pressure levels) and fracture (at high pressure levels) of the inter-particle bonds and (b) elastic and plastic deformations of the three constituent materials in the sand. The relative contributions of these two deformation mechanisms as well as their behavior are affected primarily by the degree of saturation of sand and the deformation rate. Specifically, in dry sand the first mechanism controls the sand deformation at low pressures while the second mechanism is dominant at high pressures and the effect of deformation rate is of a second order. In sharp contrast, in saturated sand very low inter-particle friction diminishes the role of the first deformation mechanism. On the other hand, the rate of deformation plays an important role. At low deformation rates, the water/air residing in the sand pores is squeezed out during deformation and, consequently, the deformation of the sand is controlled by the deformation of the solid mineral particles. At high pressures, on the other hand, water/air is trapped within the sand pores and the deformation of the sand is controlled by the deformation and the volume fractions of each of the three constituent phases.

### Equation of State

The pressure vs. density behavior of dry sand is represented using the original compaction model [21] in the form:

$$P_{dry} = \begin{cases} 0 & \rho_{dry} \leq \rho_{o,dry} \\ B_{Pl.Comp} (\rho_{dry} - \rho_{o,dry}) & \rho_{o,dry} \leq \rho_{dry} \leq \rho_{dry}^* \\ B_{SolidComp} (\rho_{dry} - \rho_s) & \rho_{dry} > \rho_{dry}^* \end{cases} \quad (5)$$

where  $B_{Pl.Comp}$  and  $B_{SolidComp}$  ( $=21.68 \text{ MPa}\cdot\text{m}^3/\text{kg}$ ) are respectively the plastic compaction (densification) and the solid-particle compaction moduli, while  $\rho_{o,dry} = (1 - \alpha_o)\rho_s$  and  $\rho_s$  ( $=2641 \text{ kg/m}^3$ ) are the initial density of dry sand and the density of the fully compacted sand, respectively and  $\alpha_o$  denotes the initial porosity in sand. It should be noted, that the compaction moduli used in Eq. (5) are defined as a ratio of the corresponding bulk moduli and mass-densities. The plastic compaction modulus,  $B_{Pl.Comp}$ , is defined as:

$$B_{Pl.Comp} = \frac{P_{Comp}}{(\rho_{dry}^* - \rho_{o,dry})} \quad (6)$$

where  $P_{Comp}$  ( $=0.6506 \text{ GPa}$ ) is the minimum pressure needed for full densification of sand and  $\rho_{dry}^*$  is given by;

$$\rho_{dry}^* = \rho_s + \frac{P_{Comp}}{B_{SolidComp}} \quad (7)$$

The pressure vs. density curve for saturated sand is taken to be rate independent and to correspond to the  $P$  vs.  $\rho$  relationship associated with a (high) deformation rate. The relationship can be expressed as:

$$P_{sat} = \begin{cases} 0 & \rho_{sat} \leq \rho_{o,sat} \\ B_{Sat}(\rho_{sat} - \rho_{o,sat}) & \rho_{sat} > \rho_{o,sat} \end{cases} \quad (8)$$

where  $B_{Sat}$  is the compaction modulus of saturated sand and is defined using the compaction modulus of solid particles,  $B_{SolidComp}$  and the compaction modulus of water,  $B_w$ , and the fact that both the solid phase and the water-filled porosity form continuous networks, as:

$$B_{Sat} = (1 - \alpha)B_{SolidComp} + \alpha B_w \quad (9)$$

while  $\rho_{o,sat}$  is the initial density of saturated sand and is defined in terms of the density of solid mineral particles,  $\rho_s$ , and the density of water,  $\rho_w$ , as:

$$\rho_{o,sat} = (1 - \alpha_o)\rho_s + \alpha_o\rho_w \quad (10)$$

The pressure vs. density curve for unsaturated sand is obtained as a linear combination of the pressure vs. density relations for the dry and the saturated sands, as:

$$P_{unsat}(\alpha_o, \beta) = \begin{cases} 0 & \rho_{unsat} \leq \rho_{o,unsat} \\ B_{unsat,low}(\rho_{unsat} - \rho_{o,unsat}) & \rho_{o,unsat} \leq \rho_{unsat} \leq \rho_{unsat}^* \\ B_{unsat,high}(\rho_{unsat} - \rho_{unsat}^*) & \rho_{unsat} > \rho_{unsat}^* \end{cases} \quad (11)$$

where

$$\rho_{o,unsat} = (1 - \beta)\rho_{o,dry} + \beta\rho_{o,sat} \quad (12)$$

$$\rho_{unsat}^* = (1 - \gamma_1)\rho_{dry}^* + \gamma_1\rho_{sat}^{(P=P_{Comp})} \quad (13)$$

$$B_{unsat,low} = \frac{P_{Comp}}{(\rho_{unsat}^* - \rho_{o,unsat})} \quad (14)$$

$$B_{unsat,high} = \left[ \frac{1}{\frac{(1 - \beta)}{B_{SolidComp}} + \frac{\beta}{B_{Sat}}} \right] \quad (15)$$

where

$$\gamma_1 = \beta \left[ \frac{1 - \frac{P_{Comp}}{B_{Sat}\rho_{sat}^*}}{(1 - \beta) \left( 1 - \frac{P_{Comp}}{B_{Pl.Comp}\rho_{dry}^*} \right) + \beta \left( 1 - \frac{P_{Comp}}{B_{Sat}\rho_{sat}^*} \right)} \right] \quad (16)$$

Eq. (15) reflects the fact that the compaction modulus of humid air residing in sand, consisting of dry air and water, is dominated by its more compliant phase (dry air).

In addition to specifying the pressure vs. density relation, the compaction model for sand entails the knowledge of the density dependence of the material's sound speed.

The material sound speed is defined as a square-root of the ratio of the bulk modulus and the material mass density. The original compaction model for sand uses the following relation for the density-dependent bulk modulus for dry sand:

$$K_{dry} = \begin{cases} 0 & \rho_{dry} < \rho_{o,dry} \\ -15.6302 + 0.0094074\rho_{dry} & \rho_{o,dry} < \rho_{dry} \leq 0.8137\rho_s \\ -93.05 + 0.0455\rho_{dry} & 0.8137\rho_s \leq \rho_{dry} \leq 0.9837\rho_s \\ -1873.3 + 0.73074\rho_{dry} & 0.9837\rho_{dry} < \rho_{dry} < \rho_s \\ -3.233 + 0.022651\rho_{dry} & \rho_{dry} > \rho_s \end{cases} \quad (17)$$

The density-dependent bulk modulus in saturated sand is derived following the same procedure as in the case of  $P_{sat}$  vs.  $\rho_{sat}$  relation as:

$$K_{sat} = B_{sat}\rho_{sat} \quad (18)$$

Likewise, the density-dependent bulk modulus for unsaturated sand is defined as:

$$K_{unsat}(\rho_{unsat}, \alpha_o, \beta) = \left[ \frac{1}{\frac{(1-\beta)}{K_{dry}(\rho_{dry})} + \frac{\beta}{K_{sat}(\rho_{sat})}} \right] \quad (19)$$

where

$$\rho_{dry} = \rho_{unsat} - \alpha_o\beta\rho_w \quad (20)$$

and

$$\rho_{sat} = \rho_{unsat} + \alpha_o(1-\beta)\rho_w \quad (21)$$

As mentioned earlier, the density dependent sound speed (for dry, saturated and unsaturated sands) is defined as a square root of the ratio of the corresponding bulk moduli and mass densities.

### *Strength Model*

Within the original compaction strength model for dry sand, the pressure dependence of yield stress is defined as:

$$\sigma_{y,dry} = \mu_{1dry}P_{dry} \approx \begin{cases} 1.3732P_{dry} & 0 < P_{dry} \leq P_{MC} \\ 1.3732P_{MC} & P_{dry} > P_{MC} \end{cases} \quad (22)$$

Also for the saturated sand, as discussed in our previous work [9], the pressure-dependent yield stress can be defined as:

$$\sigma_{y,sat} = \begin{cases} \mu_{1sat}P_{sat} & 0 \leq P_{sat} \leq P_{MC} \\ \mu_{1sat}P_{MC} & P_{sat} > P_{MC} \end{cases} \quad (23)$$

where the yield-stress-to-pressure proportionality coefficient,  $\mu_{1sat}$ , is defined as:

$$\mu_{1sat} = \begin{cases} \sqrt{3} \left( 0.1 + \frac{1.2}{\sqrt{3}} \frac{P_{sat}}{P_{MC}} \right) & 0 \leq P_{sat} \leq P_{MC} \\ 1.3732 & P_{sat} > P_{MC} \end{cases} \quad (24)$$

The term  $P_{MC}$  ( $=1.864e5$  kPa) appearing in Eqs. (22)- (24) is the Mohr-Coulomb pressure beyond which the yield stress is pressure insensitive.

The yield stress vs. pressure relationship for the unsaturated sand can then be defined using a linear combination of the yield-stress/pressure proportionality coefficients in dry and the saturated sands as:

$$\sigma_{y,sat} = \begin{cases} \mu_{1un\ sat} P_{un\ sat} & 0 \leq P_{un\ sat} \leq P_{MC} \\ \mu_{1un\ sat} P_{MC} & P_{un\ sat} > P_{MC} \end{cases} \quad (25)$$

where

$$\mu_{1un\ sat} = (1 - \beta) \mu_{1dry} + \beta \mu_{1sat} \quad (26)$$

In addition to specifying the yield stress vs. pressure relationship, the compaction strength model entails the knowledge of the density dependent shear modulus. Since water has no ability to support shear stresses, the shear modulus,  $G$ , of unsaturated sand is dominated by the shear modulus of the solid skeleton of the sand. However, the presence of water changes the density of the sand. Therefore, the original compaction shear modulus vs. density relationship defined (using ten pairs of  $(G, \rho)$  points in AUTODYN) has to be modified by adding a term  $\alpha\beta\rho_w$  to the values of density in order to obtain a (deformation-rate independent) shear modulus vs. density relationship for unsaturated sand.

### *Failure Model*

It is well established that the presence of moisture in sand increases the sand's cohesive strength [18]. Therefore, the magnitude of the (negative) failure pressure for sand is expected to increase with the saturation ratio ( $\beta$ ). Also, the moisture content should be substantial ( $\beta > 0.7$ ) before its effect on the cohesive strength of sand becomes significant [18]. To account for these two observations, in our recent work, the following expression was proposed for the magnitude of the (negative) failure pressure in unsaturated sand;  $P_{fail\ un\ sat}$ :

$$P_{fail\ un\ sat} = \beta^5 P_{fail, sat} \quad (27)$$

where  $P_{fail, sat}$  (set equal to 729kPa) is the failure pressure in saturated sand [18]. The relationship given by Eq. (27) correctly predicts that the cohesive strength of unsaturated sand with a saturation ratio of 0.7 is around 10-15% of that in the saturated sand.

### *II.4 Problem Definition and Computational Analysis*

The basic formulation of the computational problem dealing with the interactions between the detonation products, shell fragments and soil ejecta (all resulting from the explosion of a shallow-buried landmine) and the Vertical Impulse Measurement Fixture

(VIMF) is presented in this section. The computational modeling of this interaction involved two distinct steps: (a) geometrical modeling of the VIMF along with the adjoining mine, air and sand regions, and (b) the associated transient non-linear dynamics analysis of the impulse loading (momentum transfer) from the detonation products, shell fragments and soil ejecta to the VIMF structure. The part (b) of this analysis was performed using a modified version of the technique developed by Fairlie and Bergeron [19]. This technique couples a multi-material Eulerian mesh to three Lagrangian meshes. The Eulerian mesh contained initially a TNT mine (and after mine explosion the resulting high-pressure, high-internal energy-density detonation products) and the (initially stationary, atmospheric-pressure) air. The mesh was constructed in terms of eight node elements/cells. One of the Lagrangian mesh was used to model the soil, the other to represent the VIMF witness plate while the third one was used to model the remainder of the VIMF structure. The soil and the VIMF structure were modeled using eight node solid elements, while the witness plate was modeled using shell elements.

An advantage was taken of the inherit symmetry of the model. In other words, two mutually-orthogonal vertical planes of symmetry were placed along the axis of the VIMF as well as along the axis of the air, mine and sand regions which enabled only a quarter of the computational model to be analyzed. Representative quarter symmetric models for various computational domains used in the present study are shown in Fig.3. It should be noted that the lower portion of the Eulerian domain contains the landmine while the rest of the lower portion of the Eulerian domain is occupied by the Lagrangian soil mesh. Likewise, the upper portion of the Eulerian domain which extends above the soil contains initially air and is partially occupied by the Lagrangian witness plate and VIMF meshes.

Material models for air and TNT were previously defined in Section II.2.3, respectively. Both the witness plate and the VIMF structure were assigned the RHA material model which was reviewed in Section II.3.2. Welded joints of different VIMF components were simulated by joining the components in question. Sand (soil) was represented using the material model presented in Section II.3.4. The Lagrangian soil elements were allowed to erode at an incremental geometric strain of 2.0. Upon the erosion of an element, the resulting free nodes are allowed to retain their mass (and thus momentum) and to continue to interact with the soil, the witness plate and the VIMF structure.

The air/sand and air/VIMF interactions are accounted for using the appropriate Euler/Lagrange coupling option within AUTODYN [10]. Likewise, the sand/witness-plate and the sand/VIMF interactions were modeled through the use of the appropriate Lagrange/Lagrange coupling option.

The “*flow out*” boundary conditions were applied to all the free faces (the faces which do not represent interfaces between the different domains) of the Euler domain except for the face associated with the vertical symmetry planes. To reduce the effect of reflection of the shock waves at the outer surfaces of the Lagrange sand domain, “*transmit*” boundary conditions were applied to all the free faces of this domain except for the faces associated with the vertical symmetry planes and the upper face which defines the sand/air and sand/VIMF interfaces. The transmit boundary conditions enable propagation of the pressure waves across the boundaries without reflection mimicking wave propagation in an infinitely-large sand domain [21[]].

Several gage points were defined within the landmine, sand, air, witness plate and the VIMF which allowed monitoring of the quantities such as pressure, velocity and (in the case of the Lagrange domains) of the vertical displacements.

At the beginning of the simulation, all the Lagrange and Euler domains were activated and the landmine detonated. The (circular-disk shape) mine was detonated over its entire bottom face at the beginning of the simulation.

A standard mesh sensitivity analysis was carried out (the results not shown for brevity) in order to ensure that the results obtained are insensitive to the size of the cells used.

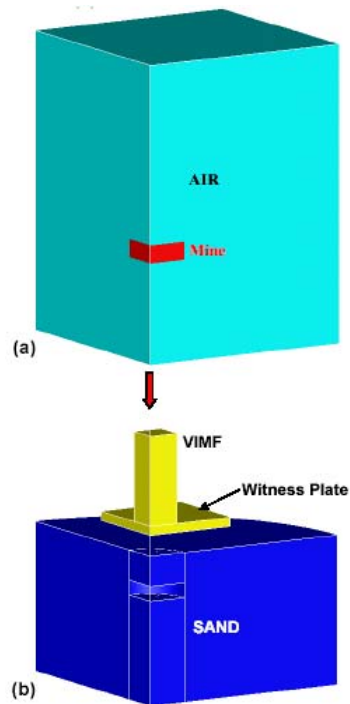


**Fig.3** Computational sub-domains used in the present work: (a) Euler sub-domain; and (b) Lagrange and Shell sub-domains.

### III. RESULTS AND DISCUSSION

#### *III.1 Validation of the Modified Compaction Model for Fully Saturated Sand*

In this section, the transient non-linear dynamics analysis described in Section II.4 is carried out in conjunction with the modified compaction material model for sand described in Section II.3.4 to examine the potential of such an analysis to quantify the blast loads resulting from detonation of the landmines buried in fully-saturated sand. This was done by comparing the model predictions for the total impulse captured by the witness plate with their experimental counterparts obtained in the work of Taylor and Skaggs [13] who carried out large-scale experiments using the Vertical Impulse

Measurement Fixture (VIMF) at the Army Research Laboratory, Aberdeen, MD. The test conditions used in the work of Taylor and Skaggs [13] are summarized in Table 1. It should be noted that two different witness plates were used with the respective length by width by thickness dimensions of 2.43m by 2.82m by 0.088m and 1.83m by 3.65m by 0.088m.

A comparison between the experimental results and their computational counterparts is given in Table 2. To demonstrate the quantitative improvements brought about by the use of the modified compaction model for sand, the corresponding computational results obtained using the original compaction model are also shown in Table 2. An examination of the results shown in this table reveals that for each of the test conditions studied by Taylor and Skaggs [13], the use of the modified compaction model for sand yields an improved agreement with the experimental findings. In some cases, e.g. test numbers 4 and 7 the agreement between the model predictions and their experimental counterparts is exceptionally good. As discussed in our previous work [12], the main two reasons for the original compaction model for sand under-predicting the magnitude of blast impulse transferred to a target structure at high saturation levels of the sand are: (a) an over-prediction of compressibility of the saturated sand which gives rise to excessive explosion-energy dissipation through irreversible compaction of the sand and (b) a lack of consideration in the original compaction model of the reduction of sand's shear strength due to moisture-induced inter-particle lubrication effects which leads to an under-prediction of the extent of sand ejection.

As mentioned earlier, the effect of sand saturation on the momentum transfer to the VIMF witness plate was carried out in our recent work [12] using a time-efficient single-material Euler-FCT model for air and detonation products. The results obtained in Ref. [12] (not repeated here for brevity) are found to be in general, higher by 5-10% than the present multi-material Euler-based results and to be in somewhat less-satisfactory agreement with the experimental results. Nevertheless, since the computational time in the case of the Euler-FCT processor are found to be lower by at least one order of magnitude, this approach appears quite acceptable at least in the early design stages of vehicles/structures which are required to withstand landmine detonation.

**Table 1** VIMF Set-Up and Test Conditions [11]

Test No.	Charge Mass kg	Charge Diameter m	Charge Height m	DoB* m	HoT** m	VIMF Target Total Mass kg
1 <sup>+</sup>	4.54	0.254	0.56	0.10	0.40	12,506
3 <sup>+</sup>	4.54	0.254	0.56	0.30	0.40	12,506
4 <sup>+</sup>	4.54	0.254	0.56	0.10	0.20	12,506
4a <sup>++</sup>	4.54	0.254	0.56	0.10	0.20	11,852
5 <sup>++</sup>	2.27	0.152	0.76	0.80	0	11,852
6 <sup>++</sup>	4.54	0.254	0.56	0.10	0.40	11,852
7 <sup>++</sup>	2.27	0.152	0.76	0.81	0.16	11,535
8 <sup>++</sup>	7.47	0.236	0.86	0.10	0.40	11,535

\* DoB = Depth of Burial

\*\* HoT = Height of the Target plate above the soil

+ Witness plate size: 2.43m by 2.82m by 0.088m

<sup>++</sup> Witness plate size: 1.83m by 3.65m by 0.088m

**Table 2** Measured and Computed Impulse Transferred to the VIMF Witness Plate

Test No.	Measured Total Impulse (N-s)	Computed Total Impulse Modified Sand Model (N-s)	Computed Total Impulse Original Sand Model (N-s)
1	71801	77470	24179
3	74017	60060	23471
4	81125	84636	26885
4a	69644	54649	22368
5	77612	71974	25251
6	59286	68196	19042
7	36938	37548	12017
8	94390	81642	29705

As discussed earlier, the hydrodynamic behavior of air was represented using an ideal gas model which may not be fully justified due to high-pressure/high-temperature conditions encountered in the vicinity of an exploded charge. To assess the effect of this choice of the materials model for air, few calculations were repeated using the real-gas Nobel-Able equation of state [22] instead of the ideal-gas equation. The results obtained (not shown here for brevity) revealed that the choice of the materials model for air had essentially a negligible effect of the momentum transferred to the witness plate. It should be also noted that the work of Raftenberg [23] clearly established that a combination of the linear equation of state and the Johnson-Cook strength and failure models like the one used in the present work can quite realistically represent the response of RHA under ballistic loading conditions. Numerous investigations [e.g.26] also showed that the Jones-Wilkins-Lee (JWL) equation of state accounts quite well for the post-detonation behavior of TNT gaseous products. With the improvements in the materials model for sand reported in this section and in our previous work [12] relative to the original compaction model for sand [21], it appears that materials models for air, structural metallic materials like RHA, high-energy explosives like TNT and sand are all at comparable levels of their ability to account for the behavior of these materials under impulse loading conditions accompanying detonation of shallow-buried and ground-laid mines.

An example of the pressure field in air during detonation of a land mine buried in the saturated sand is shown in Fig.4. For clarity, the sand and the VIMF regions of the computational domain are denoted in Figs.5 and 6 using a uniform material-specific color.

The results obtained in the present work (including the ones not shown in this paper, for brevity) clearly revealed that the momentum captured by a target (the VIMF witness plate in the present case) is greatly affected by several factors, primarily by the size of the mine, height of the target above the soil (also known as the stand-off distance), depth of burial, conditions of the soil, and size/shape of the target. Clearly, the larger is the mine the more energy is released during detonation and, with all other conditions being equal, the momentum captured by the target will scale with the mine size.

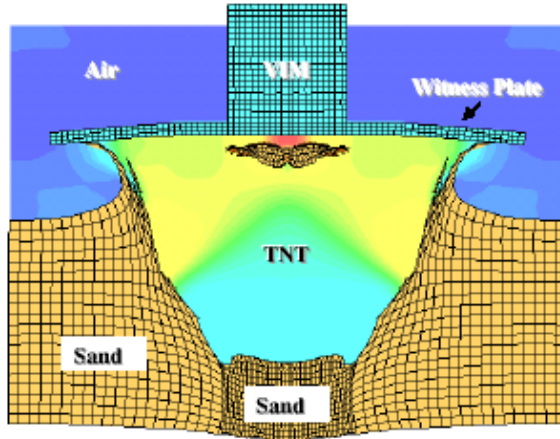


**Fig.4** An example of the pressure field in air during detonation of a mine shallow-buried in saturated sand.

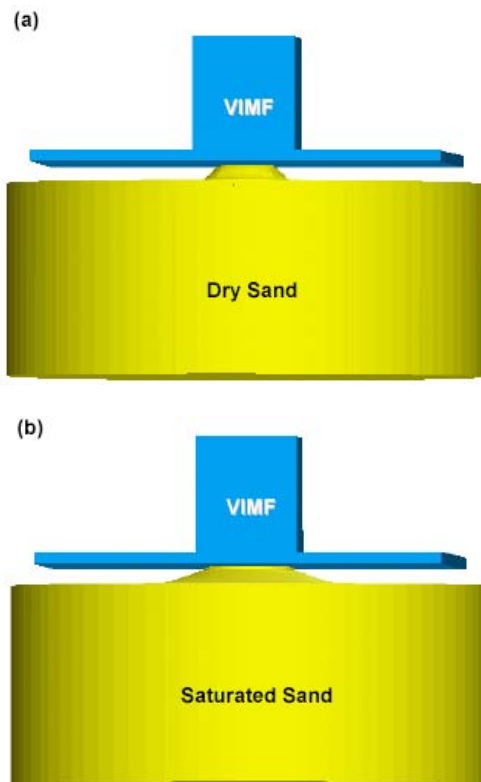


**Fig.5** Material location at a time of 0.1ms following the detonation of a 0.254m diameter and 0.055m high cylindrical disc-shaped 4.545kg TNT mine buried at a depth of 0.1m in (a) dry sand and (b) saturated sand. The witness plate standoff distance equals 0.1524m.

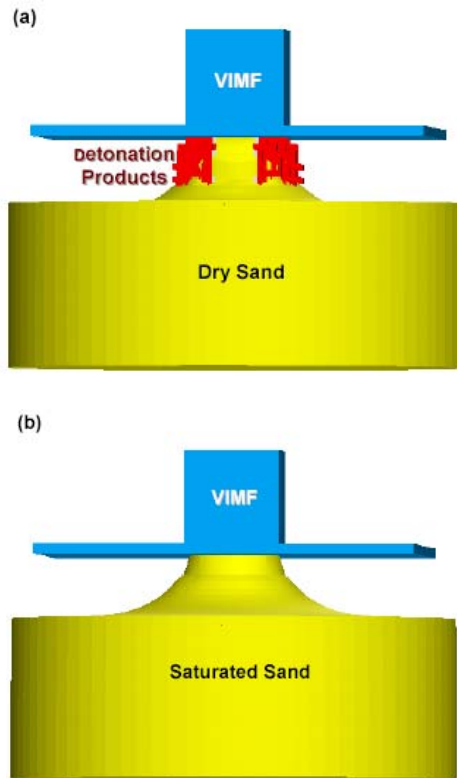


**Fig.6** Material location at a time of 0.1ms following the detonation of a 0.254m diameter and 0.055m high cylindrical disc-shaped 4.545kg TNT mine buried at a depth of 0.1m in (a) dry sand and (b) saturated sand. The witness plate standoff distance equals 0.4064m.

The stand-off distance generally plays a major role in determining the magnitude of the momentum captured by the target. If the target is ground laid (i.e. in direct contact with the soil), the shock wave from the soil will be directly transmitted into the target since the acoustic impedance mis-match between the soil and the target is relatively small. As the stand-off distance increases, the contribution of direct shock-wave transit to the target diminishes, due to a significant acoustic impedance mis-match between the air and the target. Simultaneously, greater expansion of the soil over-burden/gas bubble and a larger diameter of the ejected soil annulus accompany mine detonation [24]. The latter effects give rise to an increase in the target area over which the blast loads act, while the loads intensity decreases. The depth of burial (DOB) of a landmine generally affects both the magnitude of the momentum transferred to the target and the nature of the loading mechanism. At small DOBs, it is the gaseous detonation products that primarily carry the blast loads to the target. As the DOB increases, the detonation products are forced to push more soil upward causing the soil ejecta to make a progressively larger contribution to the momentum transfer to the target. As the mass of the ejected sand increases, its velocity is reduced and the soil impacts the target plate over a larger area. In general, the flow of the detonation products and soil ejecta becomes more directed in the upward direction as the DOB increases, since the gaseous

detonation products are constrained by crater walls from expanding in the radial and downward directions. Lastly, the condition of the soil in which the landmine is buried, particularly the level of saturation, has a significant effect on both the magnitude of the momentum transferred to the target and on the loading mechanism. At high saturation levels, the shear strength of the soil is reduced, which facilitates soil ejection [12]. In addition, saturated soils contain pores filled with water which makes its bulk modulus quite high and prevents (detonation-energy absorbing) soil compaction [20]. In other words, in the case of saturated sand, more sand is ejected and the momentum carried by the soil ejecta is larger.

### *III.2 Blast-type vs. Bubble-type Impulse Loading*

The results presented in the previous section showed clear differences in the extent of momentum transfer to the target structure for the cases of landmine detonation in dry and saturated sand (under otherwise identical other landmine detonation conditions). This finding was rationalized using the following physical phenomena/observations:

(a) Saturated sand has a lower compressibility and, hence, is capable of absorbing less of the energy released during landmine detonation;

(b) Due to an inter-particle lubrication effect of water in saturated sand, the (shear) strength of saturated sand is reduced. This in turn, gives rise to a larger extent of sand ejection (a larger crater) in the case of saturated sand. The impact of (low-compressibility) sand ejecta with the target structure, furthermore, is expected to be very effective means of transferring the detonation momentum to the target structure; and

(c) The presence of water in saturated sand increases the cohesive strength of the sand, delaying the onset of sand bubble rupture and venting of the gaseous detonation products. Due to a longer contact time between the expanding gaseous detonation products and sand, the sand will be accelerated to a greater extent and thus possess more momentum in the case of saturated sand.

In this section, additional differences in the landmine detonation in dry and saturated sand are presented. In particular, as was discussed in our previous work [12], the nature of mine detonation induced blast loading tends to be more of a shock-type in the case of dry sand and more of a bubble type in the case of saturated sand. As will be shown below, this is particularly the case for large values of the target stand-off distance.

An example of the interaction of detonation products/sand overburden with the VIMF witness plate for the case of a relatively small (0.1524m) standoff distance is shown in Figs.5 (a) and 5(b). In both cases (Fig.5 (a), pertains to the case of dry sand and Fig. 5(b) pertains to that of saturated sand) the interaction is of a bubble-type, that is, the sand overburden has bulged out but did not fracture. The momentum is, hence, transferred to the witness plate via sand overburden which is propelled, from behind, by a bubble of high pressure gaseous detonation products.

Figs.6 (a) and 6(b) show the case of witness plate blast loading but for somewhat larger value of the standoff distance (0.4064m). In the case of saturated sand, Fig.6 (b), the loading is still of a bubble type. However, in the case of dry sand, Fig.6 (a), the sand overburden has fractured causing the gaseous detonation products to vent out. At the onset of the sand-overburden burst, the air above the sand is suddenly subjected to high-pressure expanding gaseous detonation products. This interaction gives rise to formation of the shock wave which makes the witness plate loading of a shock type in this case. More precisely speaking, the witness plate in the case of dry-sand landmine detonation

is loaded with a shock wave, a blast of expanding detonation products and by sand ejecta. Furthermore, some of the detonation-products venting takes place in the radial directions, in the case of dry-sand landmine detonation, causing a lower momentum to be carried by these gasses and the sand ejecta to the witness plate.

To further reveal the differences between dry sand landmine detonation and saturated sand landmine detonation, several gages were placed in air above the sand/air interface and the pressure was monitored as a function of time at the location of the gages. An example of the results obtained for the cases of dry sand and saturated sand landmine detonation are shown in Figs.7(a)-(b), respectively. The main events such as: (a) the arrival of the first shock (the shock which was brought about by the transmission of a portion of the original shock in sand which was generated at the detonation-products/sand interface to air), at the sand/air interface; (b) the arrival of the sand-overburden and the trailing detonation-products gas bubble, and (c) the detonation-products blast and sand ejecta are clearly marked in Figs.7(a)-(b).

The main differences in the pressure vs. time traces, generated for the cases of dry sand and saturated sand landmine detonation, observed in Figs.7 (a)-(b) can be summarized as follows:

(a) While the momentum carried by the first shock wave is relatively small for both the cases of dry-sand and saturated-sand landmine detonations, the arrival time is noticeably longer in the case of dry-sand landmine detonation. This finding is consistent with the fact that due to lower speed of sound in dry-sand, the arrival of shock wave to the sand/air interface is delayed;

(b) While at short stand-off distances blast loading is of bubble-type for both dry-sand and saturated-sand landmine detonation, at higher stand-off distances blast loading resulting from landmine detonation in dry-sand involves an air-shock loading, detonation gas blast loading and sand ejecta fragments loading. In sharp contrast, blast loading is of the bubble-type in the case of saturated sand even at relatively large stand-off distances; and

(c) Peak pressures and the associated specific impulses (quantified by the area under the pressure vs. time traces) take on generally significantly lower values in the case of landmine detonation in dry-sand.

To further highlight the differences in the dry sand and saturated sand landmine detonations, the material evolution following landmine detonation is displayed in Figs. 8(a)-(c) and Figs.9(a)-(c). It is evident that in the case of dry sand, Figs.8(a)-(c), the sand overburden fractures earlier allowing venting of gaseous detonation products. In sharp contrast, Figs. 9(a)-(c) show that in the case of saturated sand, sand overburden resists fracture and produces a tunneling effect (i.e., concentration of blast load in the upward direction). It is hence generally expected to find a large momentum transferred in the case of saturated sand landmine detonation and that such momentum is focused on a smaller section of the target structure. In other words, saturated-sand landmine detonation will generally produce higher and more localized dynamic loads.

Lastly, as mentioned earlier, due to its lower compressibility, saturated sand will generally absorb a smaller fraction of the energy released during landmine detonation than dry sand. To demonstrate this fact, Figs.10(a)-(b) show a post-landmine detonation distribution of compression,  $\mu$ , in dry and saturated sand, respectively. The results displayed in these figs. clearly show that there is significantly less compression and more ejection of sand in the case of saturated sand.

In summary, through the use of transient non-linear dynamics simulations of the buried-landmine detonation and the interactions between detonation products and sand ejecta with the target structure, the main effects of moisture contents in sand have been revealed and rationalized.

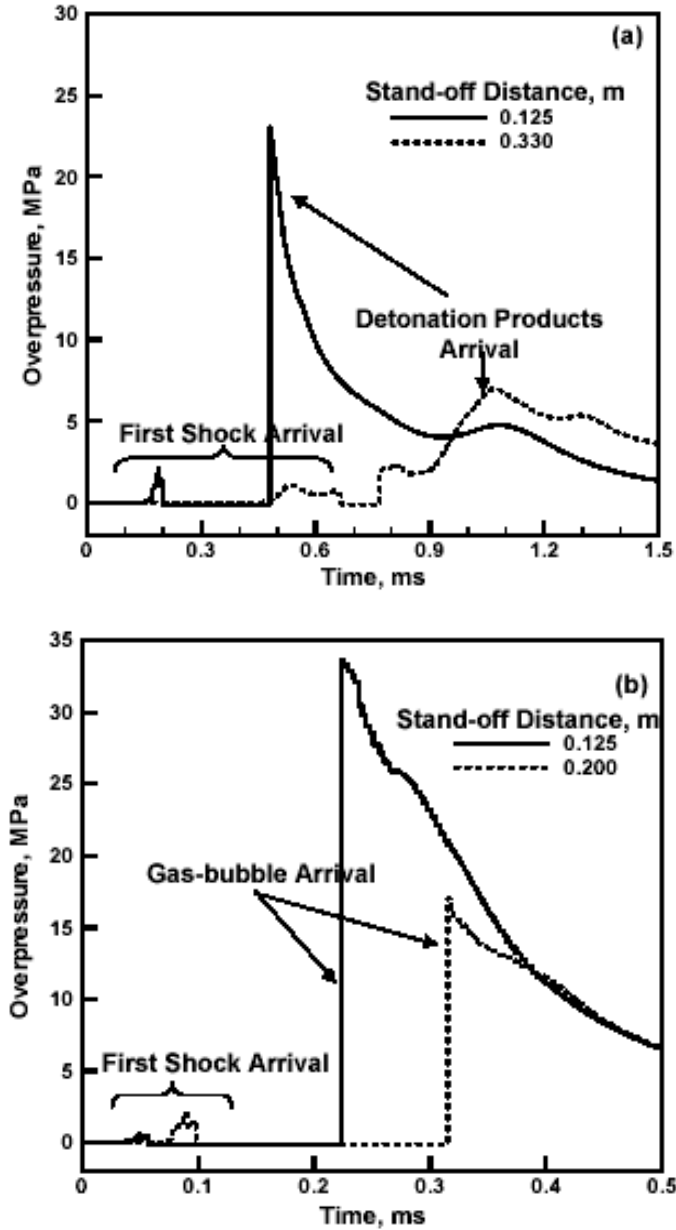


**Fig.7** Temporal evolution of pressure in air at two stand-off differences for landmine detonation in: (a) dry-sand and (b) saturated-sand.

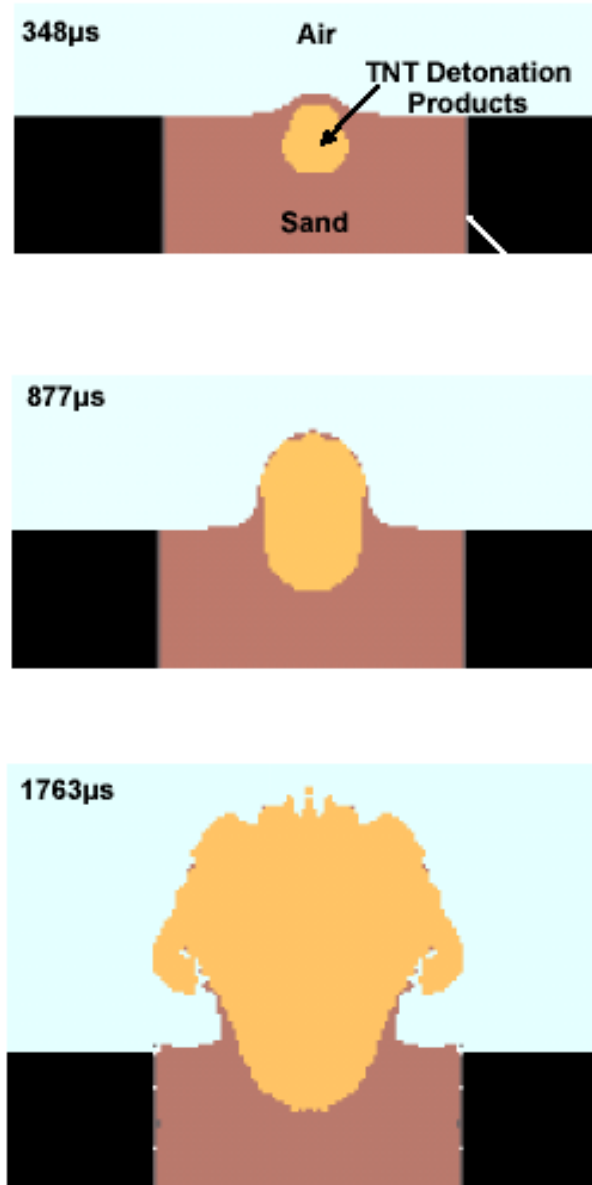


**Fig. 8** Temporal evolution of material deformation in the case of landmine detonation (DOB= 8cm) in the case of dry sand.

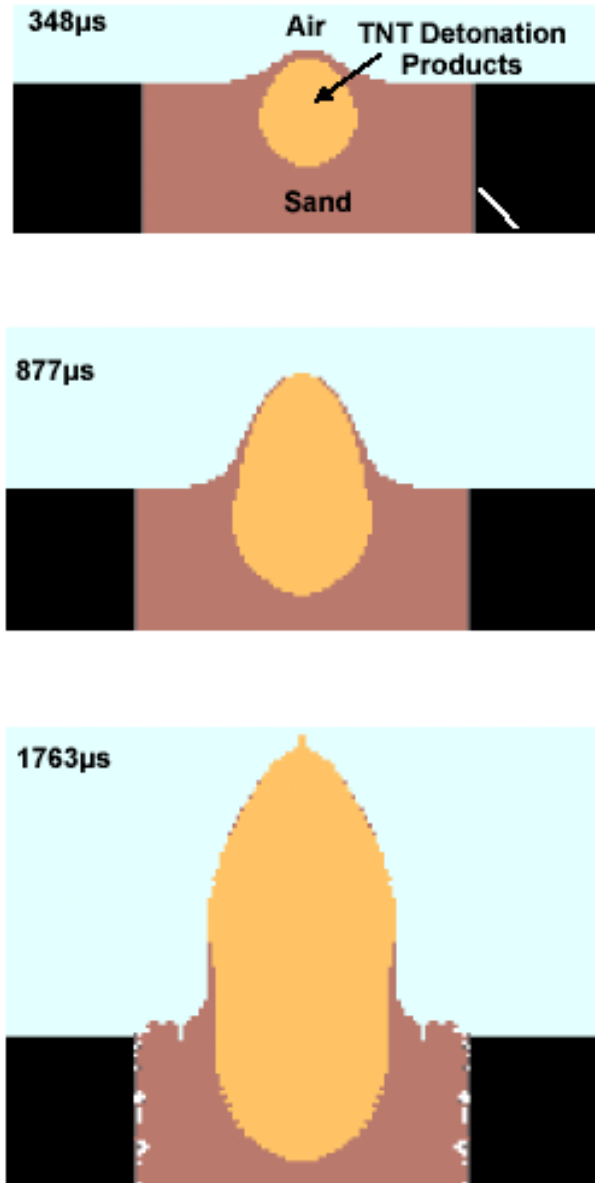


**Fig.9** Temporal evolution of material deformation in the case of landmine detonation (DOB=8cm) in the case of fully saturated sand.

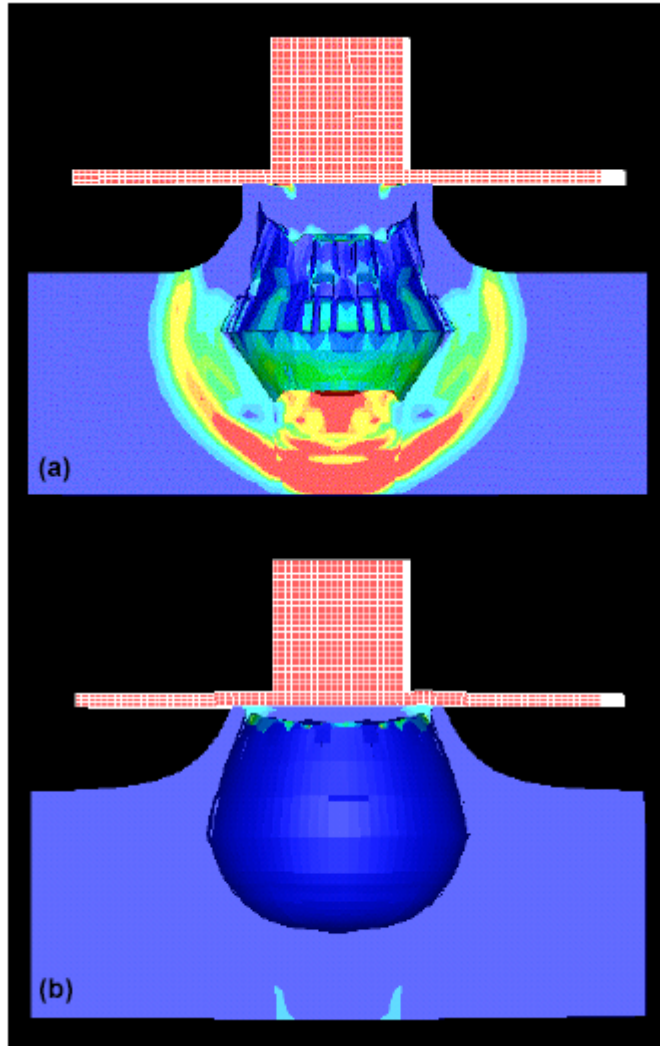


**Fig.10** Variation of sand compaction in a 0 to 0.5 range for the case of (a) dry sand and (b) saturated sand.

#### IV. SUMMARY AND CONCLUSIONS

Based on the results obtained in the present work, the following main summary remarks and conclusions can be drawn:

1. The structural-dynamics/ballistic materials model for sand recently developed by Grujicic et al. [25], which includes the effects of degree of saturation and the rate of deformation yield the momentum-transfer results which are in a significantly better

agreement (than the results obtained using original compaction model for sand) with the experimentally measured data.

2. The main deficiencies of the original compaction model for sand at high levels of saturation are found to be: (a) sand's compressibility is set too high which promotes explosion-energy dissipation through irreversible compaction of the sand; (b) a lack of consideration of the reduction of sand's shear strength brought about by a moisture-induced inter-particle lubrication effect. This shortcoming of the original compaction model for sand leads to an under-prediction of the extent of sand ejection; and (c) a lack of consideration of the increase of sand's cohesive strength brought about by a capillary-induced inter-particle cohesion effect. This deficiency of the original compaction model for sand gives rise to premature fracture of the sand over-burden and too-early venting of the high-pressure detonation products.

3. Detonation of the buried landmines in fully-saturated sand has some similarities with the under-water explosion, i.e. formation of a detonation-products bubble which propels the sand overburden appears to be the dominant momentum-transfer mode to the target structure.

## ACKNOWLEDGEMENTS

The material presented in this paper is based on work supported by the U.S. Army/Clemson University Cooperative Agreements W911NF-04-2-0024 and W911NF-06-2-0042 and by the U.S. Army Grant Number DAAD19-01-1-0661. The authors are indebted to Dr. Fred Stanton for the support and a continuing interest in the present work.

## REFERENCES

- [1]. J. E. Tremblay, D. M. Bergeron and R. Gonzalez, "Protection of Soft-Skinned Vehicle Occupants from Landmine Effects," The Technical Cooperation Program, Subcommittee on Conventional Weapons Technology, Technical Panel W-1, Key Technical Activity 1-29, August 1998.
- [2]. D. Bergeron, J. E. Tremblay, *16<sup>th</sup> International MABS Symposium*, Oxford, UK, September 2000.
- [3]. M. Grujicic, B. Pandurangan and B. Cheeseman, *Multidiscipline Model Mater. Struct.*, accepted for publication, January 2006.
- [4]. D. M. Bergeron and R. Gonzalez, "Towards a Better Understanding of Land Mine Blast Loading," The Technical Cooperation Program, Weapons Group, Conventional Weapons Technology, WPN TP-1 Terminal Effects, Key Technical Activity 1-34, June 2004.
- [5]. P. S. Westine, B. L. Morris, P. A. Cox and E. Polch, *Contract Report No. 1345, for U.S. Army TACOM Research and Development Center*, 1985.
- [6]. B. L. Morris, *Final Report for Contract No. DAAK70-92-C-0058 for the U.S. Army Belvoir RDEC, Ft. Belvoir, VA*, 1993.
- [7]. D. Bergeron, S. Hlady and M. P. Braid, *17<sup>th</sup> International MABS Symposium, Las Vegas, USA*, June 2002.
- [8]. M. P. Braid, Defence R&D Canada, Suffield Special Publication, DRES SSSP 2001-188, December 2001.
- [9]. M. Grujicic, B. Pandurangan and B. Cheeseman, *Shock and Vib.*, 13, 2006, 41-61.
- [10]. *AUTODYN-2D and 3D, Version 6.0*, User Documentation, Century Dynamics Inc., 2004.

- [11]. D. Bergeron, R. Walker and C. Coffey, "Detonation of 100-gram Anti-Personnel Mine Surrogate Charges in Sand-A Test Case for Computer Code Validation," *Suffield Report No. 668, Defence Research Establishment Suffield, Ralston, Alberta, Canada*, April 1998.
- [12]. M. Grujicic, B. Pandurangan, B. A. Cheeseman, W. N. Roy and R. R. Skaggs, *J. Mater. Design Appl.*, accepted for publication, October 2006.
- [13]. L. C. Taylor, R. R. Skaggs and W. Gault, *Fragblast*, 9(2005)19-28.
- [14]. N. Gniazdowski, "The Vertical Impulse Measurement Facility Maintenance and Inspection Manual," *ARL Technical Report* (in submission) 2004.
- [15]. R. R. Skaggs, J. Watson, T. Adkins, W. Gault, A. Canami and A. D. Gupta, "Blast Loading Measurements by the Vertical Impulse Measurement Fixture (VIMF)," *ARL Technical Report*, in submission.
- [16]. D. L. Youngs, *Numerical Methods for Fluid Dynamics*, K. W. Morton and M. J. Baines (editors), Academic Press, 1982.
- [17]. J. Henrych, "*The Dynamics of Explosion and Its Use*," Chapter 5, Elsevier Publications, New York, USA, 1979.
- [18]. D. Dowson and P. Ehret, "Past, present and future studies in elasto-hydrodynamics" *Proc. Instn. Mech. Engrs.*, 213(1999)317-333.
- [19]. G. Fairlie and D. Bergeron, *Proceedings of the 17<sup>th</sup> Military Aspects of Blast Symposium, Nevada*, June 2002.
- [20]. Z. Wang, H. Hao and Y. Lu, *Int. J. Numer. Anal. met.*, 28(2004)33-56.
- [21]. P. Laine and A. Sandvik, "Derivation of Mechanical Properties for Sand," Proceedings of the 4<sup>th</sup> Asia-Pacific Conference on Shock and Impact Loads on Structures, CI-Premier PTE LTD, Singapore, November 2001, 361-368.
- [22]. D. Schwer and K. Kailasanath, "Blast Mitigation by Water Mist (1) Simulation of Confined Blast Waves," *Report NRL/MR/6410-02-8636*, Naval Research Laboratory, Washington, August 2002.
- [23]. M. N. Raftenberg, *In. J. Impact Eng.*, 20(1997)651.
- [24]. G. M. Lyakhov, "*Principles of Dynamic Explosions in Soils and Fluid Media*", Nedra, Moscow, 1964.
- [25]. M. Grujicic, B. Pandurangan and B. Cheeseman, "A New Ballistic Material Model for Sand," *Shock and Vib.*, submitted for publication, August 2006.
- [26]. D. Bergeron, R. Walker and C. Coffey, Detonation of 100-gram Anti-Personnel Mine Surrogate Charges in Sand-A Test Case for Computer Code Validation, *Suffield Report No. 668*, Defence Research Establishment Suffield, Ralston, Alberta, Canada, April 1998.
- [27]. P. Noh and H. Woodward, "SLIC (Simple Linear Interface Calculation)," *Proceedings of the Fifth International Conference on Numerical Methods in Fluid Dynamics*, Enschede, The Netherlands, June 1976, 330-340.